Published in final edited form as:
J Phys Chem B. 2013 April 25; 117(16): 4661–4669. doi:10.1021/jp309122b.

Monitoring the Folding of Trp-cage Peptide by Two-dimensional Infrared (2DIR) Spectroscopy

Zaizhi Lai[1], **Nicholas K. Preketes**[2], **Shaul Mukamel**[2], and **Jin Wang**[1,3,4,*]

[1]Department of Chemistry, State University of New York at Stony Brook, Stony Brook, NY 11794

[2]Department of Chemistry, University of California, Irvine, Irvine, CA, 92697-2025

[3]Department of Physics and Applied Mathematics & Statistics, State University of New York at Stony Brook, Stony Brook, NY 11794

[4]State Key Laboratory of Electroanalytical Chemistry, Changchun Institute of Applied Chemistry, Chinese Academy of Sciences, Changchun, Jilin 130021, People's Republic of China

Abstract

Protein folding is one of the most fundamental problems in modern molecular biology. Uncovering the detailed folding mechanism requires methods that can monitor the structures at high temporal and spatial resolution. Two-dimensional infrared (2DIR) spectroscopy is a new tool for studying protein structures and dynamics with high time resolution. Using atomistic molecular dynamics simulations, we illustrate the folding process of Trp-cage along the dominant pathway on free energy landscape by analyzing nonchiral and chiral coherent 2DIR spectra along the pathway. Isotope-labeling is used to reveal residue-specific information. We show that the high resolution structural sensitivity of 2DIR can differentiate the ensemble evolution of protein, and thus provides a microscopic picture of the folding process.

Keywords

Protein folding; Multidimensional infrared spectroscopy; Free energy landscape; Isotope labeling

Introduction

Two-dimensional infrared (2DIR) spectroscopy [1–16] offers an effective avenue to directly reveal protein folding dynamics which accompany nanometer-scale conformational changes in the pico-to nanosecond time scale. Uncovering the folding mechanism in detail requires experimental methods for monitoring the structures with high temporal resolution. Many conventional spectroscopic methods can only provide averaged information due to the lack of high temporal resolution. For example, atomic resolution structures can be directly determined by NMR spectroscopy, but only on long approx microsecond timescales. Nanosecond measurements in NMR are based on the frequency dependence of relaxation rates and are therefore indirect.

2DIR spectroscopy achieves its time resolution through the use of femtosecond pulse sequences that interact with the protein and generate coherent nonlinear signals. The amide I band, primarily associated with the peptide bond carbonyl stretch, is the most widely studied by this technique because it is sensitive to the hydrogen bonding, dipole-dipole interactions,

*Corresponding Author: J. Wang. jin.wang.1@stonybrook.edu.

and geometry of the peptide backbone, thus providing a good indicator of secondary structure and dynamics. The cross-peaks (off-diagonal features) of the amide bands carry signatures of intra- and intermolecular couplings. Site-specific isotope-labelling, where the frequency of the amide I transition is modified by substituting $^{12}C=^{16}O$ by $^{13}C=^{16}O$ or $^{13}C=^{18}O$ can be used to spectrally isolate structurally important residues, providing site specific information on peptide folding [15]. 2DIR has been successfully applied to study many chemical and biological processes such as hydrogen bonding dynamics [17], fast chemical exchange in molecular complexes [18], and protein folding [7].

According to the current view, protein folding is envisioned to proceed along a moderately rough funnel-like energy landscape [19–28]. Many local minima in the energy landscape form due to the competition between the 'downhill' pathway towards the native state and the accumulation of misfolded and/or partially folded states. The concept of the folding pathway was originally proposed by Levinthal in 1968 [29]. Proteins do not randomly search conformational space; rather, there are biased pathways towards the folded state so that the native structure can be reached on reasonable timescales. The important issues of folding pathways have been explored from both theoretical and experimental perspectives [30–32]. Monitoring conformational changes along the pathways could shed light on the folding mechanism. Here, we generated the free energy landscape (FEL) of a fast folder Trp-cage by molecular dynamics (MD) simulations and observed the conformational evolution on the folding pathway through 2DIR spectroscopy.

The 2DIR signal is generated by three laser pulses with wavevectors $\mathbf{k}_1$, $\mathbf{k}_2$, and $\mathbf{k}_3$. The coherent signal field is emitted along the phase-matching directions $\mathbf{k}_4=\pm\mathbf{k}_1\pm\mathbf{k}_2\pm\mathbf{k}_3$ and is heterodyne-detected by interference with a fourth 'local-oscillator' pulse with wavevetor $\mathbf{k}_4$. The pulses interact with the protein and produce a coherent nonlinear signal which depends on three time delays $S(t_3, t_2, t_1)$. A two-dimensional Fourier transform generates a 2DIR spectrum $S(\Omega_3, t_2, \Omega_1)$, where Ω_3 and Ω_1 are the frequency conjugates to t_3 and t_1, respectively. By choosing different polarization configurations, one can obtain non-chiral (i.e. *xxxx*) and chirality-induced (CI) (i.e. *xxxy*) signals [4], where *ijkl* represents the polarization configuration of the four pulses in chronological order. Although CI 2DIR spectroscopy has not yet been implemented experimentally as the signal fields are 3 to 4 orders of magnitude weaker than nonchiral 2DIR signals, the cross peaks in the CI 2D signals are explicitly coordinate-dependent and are therefore particularly sensitive to structural changes. CI 2DIR and CI 2D ultraviolet spectra have been predicted for proteins using QM/MM simulations [2, 3, 33–37].

In this computational study, we demonstrate how 2DIR spectroscopy may be used to monitor the ultrafast folding process of the 20-residue Trp-cage peptide (Asn1-Leu2-Tyr3-Ile4-Gln5-Trp6-Leu7-Lys8-Asp9-Gly10-Gly11-Pro12-Ser13-Ser14-Gly15-Arg16-Pro17-Pro18-Pro18-Ser20), which is one of the fastest folding mini-proteins. Although Trp-cage is small and relatively simple, the mechanism of its folding remains elusive. Some studies [38, 39] have suggested that it follows a simple two-state folding mechanism. On the other hand, recent UV-resonance raman experiments [40] show that Trp-cage is not a simple two-state miniprotein. Additionally, the folding time determined by tryptophan fluorescence and recent 2D ^{1}H NMR spectra experiment suggests downhill folding mechanism [27]. It is very interesting that even for such a small system we still have conflicting views of its folding mechanism. 2DIR spectra may provide a detailed picture of the structure and dynamics of the peptide along the pathway and the folding mechanism.

Methods

Molecular dynamics (MD) simulations

All MD simulations were carried out using the AMBER 10 software package [41] with AMBER ff99SB protein force field [42]. It has been reported that the folding temperature for Trp-cage is in the range 313–317K [27]. The constant temperature of 315K was maintained in our simulations by assigning atom velocities from a Gaussian distribution for the different trajectories [43]. 50 200-ns trajectories were simulated. The initial structure is given by a extended conformation. An implicit solvation model [44] with the collision frequency of 1 ps^{-1} was applied in the MD simulations. The SHAKE algorithm [45] was used to constrain covalent bonds involving hydrogen atoms. A timestep of 2 fs was used. These 50 trajectories covering total 10 μs simulations of peptide folding, provide enough data for constructing the FEL. Several locations were harvested along the dominant folding pathway from the unfolded to the folded state, to calculate the IR signals.

Calculation of 2DIR spectra

Using the bosonic creation and annihilation operator of a vibrational exciton $B_i^\dagger$ and B_i, the effective vibrational Hamiltonian of the system is [3]:

$$H(t)=\sum_i \hbar\omega_i(t)B_i^\dagger B_i+\sum_{ij}\hbar J_{ij}(t)B_i^\dagger B_j-\sum_{ij}\frac{\hbar\Delta_i}{2}B_i^{\dagger 2}B_i^2 \quad (1)$$

where $\omega_i(t)$ is the fundamental frequency of the local mode i, $J_{ij}(t)$ represents the coupling between modes i and j, and Δ_i is the anharmonicity of mode i. The coupling between the system and the electric field $\boldsymbol{E}(t)$ of the laser pulses is:

$$H'(t)=\sum_i \boldsymbol{\mu_i}(t)\cdot\mathbf{E}(t)(B_i^\dagger+B_i) \quad (2)$$

where $\mu_i(t)$ is the transition dipole of the i^{th} mode.

We have used electrostatic existing DFT maps to evaluate the fluctuating parameters in $H(t)$ and $H'(t)$ for the amide I vibrations. The electrostatic DFT map of [46] was used to evaluate $\omega_i(t)$ while the transition dipole was fixed to the gas phase value [47] and the anharmonicity was fixed to the measured value of −16 cm^{-1} [48]. The field free frequency of the DFT map was set to 1670 cm^{-1} to obtain reasonable agreement with experiment [49]. J_{ij} was given by the transition-dipole coupling model [50].

Absorptive 2DIR spectra were simulated for non-chiral (*xxxx*) and CI (*xxxy*) polarization configurations after constructing the vibrational Hamiltonian (Eqn. 1). Absorptive signals are defined as the addition of the rephasing ($\mathbf{k}_I=-\mathbf{k}_1+\mathbf{k}_2-\mathbf{k}_3$) and non-rephasing ($\mathbf{k}_{II}=\mathbf{k}_1-\mathbf{k}_2+\mathbf{k}_3$) spectra. All signals were calculated in the inhomogeneous limit by averaging over 200 configurations extracted from each location on the FEL. Homogeneous broadening was set to 5.5 cm^{-1} for all transitions. For each snapshot, the implicitly solvated peptide was explicitly resolvated with TIP3P water model [51] and equilibrated for 10 ps. The explicitly solvated and equilibrated structure was used to compute all signals. We assumed short impulsive pulses and $t_2 = 0$. The 2DIR spectra were computed using the quasiparticle approach based on the nonlinear exciton equations [52–55], as implemented in SPECTRON [56].

Results and Discussion

Folding Mechanism

Fig. 1 shows the FEL vs the root mean square deviation (RMSD) from the folded structure and the radius of gyration (R_g). The FEL was determined by calculating $F = -\log(P)$, where P is the population obtained from the 10 μs MD simulated data, including 50 MD trajectories of 200 ns each.

The FEL reveals several interesting features of the folding mechanism. First, it is fairly smooth and there are no apparent thermodynamic barriers or intermediate states, implying that it may follow a downhill folding mechanism. In addition, there is an obvious dominant pathway connecting the unfolded to the folded state (black curve in Fig. 1). We have calculated the 2DIR spectra at five locations along the folding pathway, L1, L25, L50, L75, and L100. From L1 to L25, the peptide structure does not change significantly and retains the extended linear or coil structure. After the peptide reaches L50, the folding process seems to accelerate and the peptide rapidly reaches the folded state.

To demonstrate the structural changes that occur during folding, we display the transition dipole couplings between residues in Fig. 2. At both L1 and L25, the couplings are weak and primarily nearest-neighbor. This is indicative of the random coil structure at these locations. At L50, the α-helix extending from residues 2 to 9 has formed as seen by the strong positive nearest neighbor coupling and the strong negative 1–3 coupling in this region [11]. The same coupling pattern was observed in simulations of the Villin headpiece, which contains three α-helices [11]. At L75, we observe the formation of the short 3_{10}-helix-like structure from residues 11 to 14. This can be seen by the strong positive nearest-neighbor coupling in this region. At L100, the system has reached the native state and we see the N-terminal α-helix and the 3_{10}-helix-like structure from residues 11 to 14. In Fig. 3, we present the couplings between the α-helix region (residues 1–9) and the coil region (residues 15–19), which are much weaker than the intra-helical or intra-coil couplings. There is almost no coupling between these two groups at L1 and L25 (Fig. 3). At L50, the two groups become strongly coupled. However, at L75, the coupling between these two groups changes, indicating an orientational rearrangement. Comparing L75 and L100, the coupling pattern remains largely the same, however, with larger magnitudes. This indicates that the structural changes between L75 and L100 involves only minor rearrangements.

To further characterize the folding process, we had calculated the average number of hydrogen bonds at each location to illustrate the folding process (Table 1). Between L25 and L50, the number of hydrogen bonds in the entire peptide and particularly the α-helix region abruptly increases. The increase in the number of α-helix hydrogen bonds is largely caused by the increasing number of inter-α-helix rather than intra-α-helix hydrogen bonds. At the same time, the number of hydrogen bonds in the coil region shows a large increase while the number of hydrogen bonds in the “other” region only increases slightly. These observations suggest that the α-helix tends to form hydrogen bonds with the coil region to form a “two-strand” structure between L25 and L50. This is consistent with the analysis of transition dipole coupling in Fig. 3 which shows no coupling between the “two strands” (N-terminal α-helix region and C-terminal coil region) at L1 and L25 but strong coupling after L50. The formation of this “two-strand” structure can dramatically reduce the conformational searching in the huge configuration space and help the peptide fold into its correct native structure. After L50, the number of intra-α-helix hydrogen bonds continues to increase smoothly, implying the growth of the α-helix. Interestingly, the number of inter-α-helix hydrogen bonds decreases when moving from L50 to L100, indicating that residues 1–9 tend to form hydrogen bonds among themselves, outcompeting the inter-α-helix hydrogen bonds as the α-helix gradually grows.

2DIR Snapshots of Peptide Folding

In all simulations, unless specified otherwise, we consider an isotopomer of Trp-cage where Trp6 and Pro18, which is an important link that stabilizes the native state [58], are $^{13}C=^{18}O$ isotope labeled. To account for the isotope-labeling, the field free frequency of the isotope-labeled amide I modes was red-shifted by 65 cm^{-1} compared to the unlabeled modes [3]. The double isotope-labeling scheme was used to obtain information on the local dynamics of Trp6 and Pro18, which are on opposite "strands" of the peptide. Therefore, their coupling may provide information on the formation of the tertiary structure of the peptide.

Fig. 4(a) shows the amide I absorption spectra at the five FEL locations. The amide I absorption of the unlabeled group results in a single peak, whose maximum red-shifts from 1650 cm^{-1} at L1 and L25 to 1640 cm^{-1} at L100. The 10 cm^{-1} redshift is consistent with recent time-resolved IR experiments on Trp-cage [59]. This is due to the formation of the secondary structure and hydrogen bonds, as shown in Table 1, which weakens the C=O bond and reduces its vibrational frequency [5]. The peak intensity decreases from L1 to L50 and then increases from L50 to L100, which indicates that ordered structures, including the linear extended structure and folded structures, tend to enhance the intensity.

Since the contributions from the isotope-labeled residues are much weaker than those from the unlabeled residues, we enlarge the spectral region corresponding to isotope-labeled amide I modes in Fig. 4(b)–(f). There are two bands in the isotope-labeled region of the linear absorption spectrum. One is near 1560–1570 cm^{-1}, and the other is around 1580–1590 cm^{-1}. To determine the origins of these two bands, we have calculated the projected density of states [11]:

$$\rho_i(\omega)=\sum_{\lambda}\left\langle \left|\Psi_{i,\lambda}\right|^2\delta(\omega-\omega_i)\right\rangle \quad (3)$$

where $\Psi_{i,\lambda}$ is the component of the exciton eigenstate λ on the site *i* and ω_λ is the λ^{th} eigenvalue. The projected density of states shows that the higher frequency band in the isotope-labeled region originates from Pro18 while the lower frequency band originates from Trp6, as shown in Fig. 4(b)–(f).

The absorptive 2DIR *xxxx* spectra are displayed in Fig. 5. All spectra are dominated by an inhomogeneously (diagonally) broadened peak centered near (−1640, 1640) cm^{-1}. The peak shape is largely determined by the inhomogeneous distribution and the homogeneous dephasing of 5.5 cm^{-1} which were used to compute the spectra. The diagonal L100 peak is red-shifted by ≈10 cm^{-1} compared to L1, consistent with the above linear absorption spectrum and the previous study [14]. The similarity of the 2DIR *xxxx* spectra of the unlabeled amide groups indicates that the *xxxx* signals are not very sensitive to protein secondary structure motifs without the use of site-specific isotope-labeling.

The 2DIR *xxxx* spectra in the region of the isotope labeled residues shows some interesting features during folding (Fig. 5). Starting at L50, two isotope-labeled bands clearly begin to emerge at approximately (−1570,1570) cm^{-1} and (−1590,1590) cm^{-1}. The band around (−1570,1570) cm^{-1} gradually increases from L50 to L100 and the intensities of the band around 1590 cm^{-1} are almost unchanged from L50 to L100. After the two bands appear at L50, the cross peak at (−1570 cm^{-1}, 1590 cm^{-1}) emerges. At L1 and L25, this cross peak is extremely weak and the coupling between the two isotope-labeling residues is nearly zero, as shown in Fig. 6. At L50, the magnitude of the coupling increases by nearly an order of magnitude while the cross peak intensity also increases. Between L50 to L100, both the coupling and the cross peak intensity continue to increase. It should be noted that the couplings at L50 and L75 have both positive and negative values due to the varying relative

orientation between Trp6 and Pro18, while at L100, the coupling is always positive as the relative orientation of the two strands has been stabilized.

The vibrational circular dichroism (VCD) and CI 2DIR spectra are shown in Figs. 7 and 8, respectively. The unlabeled amide I band in the VCD spectra has one negative and one positive peak (Fig. 7(a)). However, these peaks are red-shifted as the peptide moves from L1 to L100. At L25, the VCD signal nearly vanishes due to the cancellation of various random coil configurations upon ensemble averaging. After the formation of the compact form at L50, the VCD intensity ascends from L50 to L100.

The isotope-labeled band of the VCD spectra is shown for three different isotopomers in Fig. 7(b)–(d). To determine the contributions of Trp6 and Pro18 to the VCD spectrum, we calculated the VCD spectra of the isotopomers where only Trp6 (Fig. 7c) or Pro18 (Fig. 7d) are labeled. In the double-labeled spectrum (Fig. 7(b)), the peak is redshifted from 1600 cm^{-1} at L1 to 1565 cm^{-1} at L100. At L50, L75, and L100, the single-labeled spectra of Trp6 closely resemble the double-labeled spectra, demonstrating that Trp6 dominates the double-labeled spectrum after L50. However, at L1 and L25, the double-labeled spectra is dominated by the contribution of Pro18, resulting in a peak at ≈1590–1600 cm^{-1}.

The absorptive *xxxy* signals of the five states are displayed in Fig. 8. There are two types of chirality in proteins. One is related to global structure and the other is associated with the local chirality originating from the individual vibrational modes. We only consider the former because it dominates the response in extended systems [4].

The *xxxy* spectra (Fig. 8) show two inhomogeneously broadened diagonal peaks that are surrounded by four symmetricially distributed cross peaks. The stronger diagonal peak is initially located at (−1645,1645) cm^{-1} and redshifts to (−1630,1630) cm^{-1} during folding, while the weaker peak is initially located at (−1625,1625) cm^{-1} and redshifts to (−1610,1610) cm^{-1}. Both peaks contain contributions from several highly delocalized transitions which cannot be assigned to specific sites. The cross peak of these two transitions is seen at approximately (−1620,1645) cm^{-1} and is related to the coupling between these two classes of delocalized transitions. We note that in the non-chiral spectra, there was only a single diagonal peak for the unlabeled amide I band, presenting an obvious advantage for CI 2DIR.

During folding, the cross peaks are also red-shifted along the diagonal, similar to the diagonal peaks. At L1 and L25, the four cross peaks are weak When the peptide evolves to L50, the intensities of the four cross peaks increase due to the increased copuling caused by the relatively compact conformation. After L50, the peak locations remain similar while the intensities of the four cross peaks increase (Fig. 8(d) and (e)). The increase in the intensities of the cross peaks is caused by the increased coupling between residues (Fig. 2).

Another interesting feature is the isotope-labeled band around 1560–1590 cm^{-1}. At L1 and L25, this band is extremely weak due to the cancellation of contributions from various random coil configurations, as in the VCD spectra. After L50, a weak band appears that gradually enhances and red-shifts as the peptide folds, indicating that the two isotope-labeled residues, Trp6 and Pro18, get close to each other and maintain a particular relative orientation from L75 to L100.

Hamm *et al.* had measured 2DIR signals of a photoswitchable isotope-labeled α-helix [9] whose structure is very similar to Trp-cage in the folded state. Our simulation results are consistent with their findings for the changes between the folded and unfolded conformations. They also found two bands for some residues in the isotope-labeled region. Note that the folding time scale in our simulations is not necessary the real experimental

folding time scale since the Generalized Born solvent model was applied to run the simulations and this implicit solvent model reduced the folding time dramatically. Nevertheless, the conformational transition of the folding process and corresponding spectrum changes are our main concern, and the implicit solvent model and spectrum calculations have proven to give reasonable results in previous studies [4, 11, 44].

Conclusions

We have demonstrated that valuable conformational information about the structural evolution on the folding pathway can be revealed by multidimensional IR spectroscopy. The folding of a 20-residue peptide was simulated to build up the FEL which suggests one dominant pathway that connects the unfolded and native state. The amide I absorption, VCD, non-chiral, and CI 2DIR spectra were simulated to structurally illustrate the characters of the folding process. The spectra were calculated for an isotopomer where Trp6 and Pro18 were $^{13}C=^{18}O$ labeled. The linear absorption spetra shows a 10 cm^{-1} redshift of the unlabeled amide I band, consistent with experimental results. In the isotope-labeled region of the linear absorption, there are two peaks around 1560 cm^{-1} and 1590 cm^{-1}, which are caused by Trp6 and Pro18, respectively. The diagonal peak of the unlabeled amide I band in the 2DIR *xxxx* spectrum redshifts 10 cm^{-1} during folding. The cross peak intensity between the $^{13}C=^{18}O$ labeled Trp6 and Pro18 amide I transitions increases during folding. The intensity of this cross-peak is correlated with the coupling between these two groups and is indicative of the formation of the peptide's tertiary structure, which is consistent with the analysis of transition dipole coupling and hydrogen bonds. The VCD spectra revealed two peaks for the unlabeled amide I band which were redshifted during folding. The overall intensity of the VCD spectra increased during folding because the cancellation of various random coil conformations upon ensemble averaging of the signal. The isotope-labeled band revealed two peaks around 1560 cm^{-1} and 1600 cm^{-1} which were redshifted, similar to the linear absorption. The CI 2DIR spectra showed two distinct diagonal peaks for the unlabeled amide I band, whereas the non-chiral spectra only showed a single diagonal peak in this region. Strengthening of the cross peaks of the unlabeled amide I band was observed during folding which is directly correlated with the increase in coupling. While CI 2DIR experiments have yet to be performed, our simulations show that CI 2DIR measurements may reveal changes in cross peaks which may be difficult to see in non-chiral 2DIR measurements.

Acknowledgments

The research leading to these results has received funding from the National Institutes of Health (grants GM059230 and GM091364) and the National Science Foundation (grant CHE-1058791). N.K.P. is supported by a National Science Foundation Graduate Research Fellowship. Z.Z.L. and J.W. thank National Science Foundation and National Institutes of Health for support.

References

1. Mukamel S, Abramavicius D. Many-Body Approaches for Simulating Coherent Nonlinear Spectroscopies of Electronic and Vibrational Excitons. Chem. Rev. 2004; 104:2073–2098. [PubMed: 15080721]
2. Zhuang W, Sgourakis NG, Li Z, Garcia AE, Mukamel S. Discriminating Early Stage Aβ42 Monomer Structures Using Chirality-Induced 2DIR Spectroscopy in a Simulation Study. Proc. Natl. Acad. Sci. 2010; 107:15687–15692. [PubMed: 20798063]
3. Zhuang W, Hayashi T, Mukamel S. Coherent Multidimensional Vibrational Spectroscopy of Biomolecules; Concepts, Simulations and Challenges. Angew. Chem. Int. Ed. 2009; 48:3750–3781.
4. Zhuang W, Abramavicius D, Mukamel S. Two-Dimensional Vibrational Optical Probes for Peptide Fast Folding Investigation. Proc. Natl. Acad. Sci. 2006; 103:18934–18938. [PubMed: 17146054]

5. Xiang Y, Duan LL, Zhang JZH. Folding Dynamics of A Small Protein at Room Temperature via Simulated Coherent Two-Dimensional Infrared Spectroscopy. Phys. Chem. Chem. Phys. 2010; 12:15681–15688. [PubMed: 20676442]
6. Moran AM, Park SM, Dreyer J, Mukamel S. Linear and Nonlinear Infrared Signatures of Local α- and 3_{10}-Helical Structures in Alanine Polypeptides. J. Chem. Phys. 2003; 118:3651–3659.
7. Chung HS, Ganim Z, Jones KC, Tokmakoff A. Transient 2D IR Spectroscopy of Ubiquitin Unfolding Dynamics. Proc. Natl. Acad. Sci. 2007; 104:14237–14242. [PubMed: 17551015]
8. Wang L, Middleton T, Zanni MT, Skinner JL. Development and Validation of Transferable Amide I Vibrational Frequency Maps for Peptides. J. Phys. Chem. B. 2011; 115:3713–3724. [PubMed: 21405034]
9. Backus EHG, Bloem R, Donaldson PM, Ihalainen JA, Pfister R, Paoli B, Caflisch A, Hamm P. 2D-IR Study of a Photoswitchable Isotope-Labeled alpha-Helix. J. Phys. Chem. B. 2010; 114:3735–3740. [PubMed: 20166694]
10. Smith AW, Lessing J, Ganim Z, Chunte SP, Tokmakoff A. Melting of a β-Hairpin Peptide Using Isotope-Edited 2D IR Spectroscopy and Simulations. J. Phys. Chem. B. 2010; 114:10913–10924. [PubMed: 20690697]
11. Bagchi S, Falvo C, Mukamel S, Hochstrasser RM. 2D-IR Experiments and Simulations of the Coupling between Amide-I and Ionizable Side Chains in Proteins: Application to the Villin Headpiece. J. Phys. Chem. B. 2009; 113:11260–11273. [PubMed: 19618902]
12. Marai CNJ, Mukamel S, Wang J. Probing the Folding of Mini-Protein Beta3s by Two-Dimensional Infrared Spectroscopy: Simulation Study. PMC Biophysics. 2010; 3:8. [PubMed: 20302645]
13. Demirdoven N, Cheatum CM, Chung HS, Khail M, Knoester J, Tokmakoff A. Two-Dimensional Infrared Spectroscopy of Antiparallel β-Sheet Secondary Structure. J. Am. Chem. Soc. 2004; 126:7981–7990. [PubMed: 15212548]
14. Ganim Z, Chung HS, Smith AW, DeFlores LP, Jones KC, Tokmakoff A. Amide I Two-Dimensional Infrared Spectroscopy of Proteins. Acc. Chem. Res. 2008; 41:432–441. [PubMed: 18288813]
15. Roy S, Jansen TLC, Knoester J. Structural Classification of the Amide I Sites of a β-Hairpin with Isotope Label 2DIR Spectroscopy. Phys. Chem. Chem. Phys. 2010; 12:9347–9357. [PubMed: 20596553]
16. Zanni MT, Gnanakaran S, Stenger J, Hochstrasser R. Heterodyned Two-Dimensional Infrared Spectroscopy of Solvent-Dependent Conformations of Acetylproline-NH2. J. Phys. Chem. B. 2001; 105:6520–6535.
17. Jansen C, Dijkstra AG, Watson TM, Hirst JD, Knoester J. Modeling the Amide I Bands of Small Peptides. J. Chem. Phys. 2006; 125:044312.
18. Finkelstein IJ, Zheng JR, Ishikawa H, Seongheun Kim S, Kwak K, Fayer MD. Probing Dynamics of Complex Molecular Systems with Ultrafast 2D IR Vibrational Echo Spectroscopy. Phys. Chem. Chem. Phys. 2007; 9:1533–1549. [PubMed: 17429547]
19. Levy Y, Wolynes PG, Onuchic JN. Protein Topology Determines Binding Mechanism. Proc. Natl. Acad. Sci. USA. 2004; 101:511–516. [PubMed: 14694192]
20. Shoemaker BA, Portman JJ, Wolynes PG. Speeding Molecular Recognition by Using the Folding Funnel: The Fly-Casting Mechanism. Proc. Natl. Acad. Sci. USA. 2000; 97:8868–8873. [PubMed: 10908673]
21. Lai ZZ, Lu Q, Wang J. Exploring the Thermodynamic Landscape, Kinetics, and Structural Evolution of a Protein Conformational Transition with a Microscopic Double-Well Model. J. Phys. Chem. B. 2011; 115:4147–4159. [PubMed: 21425801]
22. Papoian GA, Wolynes PG. The Physics and Bioinformatics of Binding and Folding-an Energy Landscape Perspective. Biopolymers. 2003; 68:333–349. [PubMed: 12601793]
23. Karplus M. Behind the Folding Funnel Diagram. Nature Chemical Biology. 2011; 7:648.
24. Wang J, Verkhivker GM. Energy Landscape Theory, Funnels, Specificity, and Optimal Criterion of Biomolecular Binding. Phys. Rev. Lett. 2003; 90:188101. [PubMed: 12786043]
25. Lai ZZ, Su JG, Chen WZ, Wang CX. Uncovering the Properties of Energy-Weighted Conformation Space Networks with a Hydrophobic-Hydrophilic Model. Int. J. Mol. Sci. 2009; 10:1808–1823. [PubMed: 19468340]

26. Xu WX, Lai ZZ, Oliveira RJ, Leite VBP, Wang J. Configuration-Dependent Diffusion Dynamics of Downhill and Two-State Protein Folding. J. Phys. Chem. B. 2012; 116:5152–5159. [PubMed: 22497604]
27. Halabis A, Zmudzinska W, Liwo A, Oldziej S. Conformational Dynamics of the Trp-Cage Miniprotein at Its Folding Temperature. J. Phys. Chem. B. 2012; 116:6898–6907. [PubMed: 22497240]
28. Zhou RH. Trp-cage: Folding Free Energy Landscape in Explicit Water. Proc. Natl. Acad. Sci. USA. 2003; 100:13280–13285. [PubMed: 14581616]
29. Levinthal, C. How to Fold Graciously. In: Debrunner, P.; Tsibris, J.; Munck, E., editors. Proceedings in Mossbauer Spectroscopy in Biological Systems. Illinois: University of Illinois press; 1969. p. 22
30. Wang J, Onuchic JN, Wolynes PG. Statistics of Kinetic Pathways on Biased Rough Energy Landscapes with Applications to Protein Folding. Phys. Rev. Lett. 1996; 76:4861. [PubMed: 10061399]
31. Kiefhaber T. Kinetic Traps in Lysozyme Folding. Proc. Natl. Acad. SciU.S.A. 1995; 92:9029.
32. Dyson HJ, Wright PE. Unfolded Proteins and Protein Folding Studied by NMR. Chem. Rev. 2004; 104:3607–3622. [PubMed: 15303830]
33. Abramavicius D, Mukamel S. Coherent Third-Order Spectroscopic Probes of Molecular Chirality. J. Chem. Phys. 2005; 122:134305. [PubMed: 15847463]
34. Zhuang W, Abramavicius D, Mukamel S. Two-Dimensional Vibrational Optical Probes for Peptide Fast Folding Investigation. Proc. Natl. Acad. Sci. 2006; 103:18934. [PubMed: 17146054]
35. Jiang J, Mukamel S. Probing Amyloid Fibril Growth by Two-Dimensional Near-Ultraviolet Spectroscopy. J. Phys. Chem. B. 2011; 115:6321–6328. [PubMed: 21517033]
36. Jiang J, Mukamel S. Two-Dimensional Near-Ultraviolet Spectroscopy of Aromatic Residues in Amyloid Fibrils: a First Principles Study. Phys. Chem. Chem. Phys. 2011; 13:2394–2400. [PubMed: 21132201]
37. Lam A, Jiang J, Mukamel S. Distinguishing Amyloid Fibril Structures in Alzheimer's Disease (AD) by Two-Dimensional Ultraviolet (2DUV) Spectroscopy. Biochem. 2011; 50:9809–9816. [PubMed: 21961527]
38. Neidigh JW, Fesinmeyer RM, Andersen NH. Designing a 20-Residue Protein. Nat. Struct. Biol. 2002; 9:425–430. [PubMed: 11979279]
39. Gellman SH, Woolfson DN. Mini-Proteins Trp the Light Fantastic. Nat. Struct. Biol. 2002; 9:408–410. [PubMed: 12032551]
40. Ahmed Z, Beta IA, Mikhonin AV, Asher SA. UV-Resonance Raman Thermal Unfolding Study of Trp-Cage Shows That It Is Not a Simple Two-State Miniprotein. J. Am. Chem. Soc. 2005; 127:10943–10950. [PubMed: 16076200]
41. Case, DA.; Darden, TA.; Cheatham, TE., III; Simmerling, CL.; Wang, J.; Duke, RE.; Luo, R.; Crowley, M.; Walker, RC.; Zhang, W., et al. AMBER 10. University of California; San Francisco: 2008.
42. Hornak V, Abel R, Okur A, Strockbine B, Roitberg A, Simmerling C. Comparison of Multiple Amber Force Fields and Development of Improved Protein Backbone Parameters. Proteins. 2006; 65:712–725. [PubMed: 16981200]
43. Leach, AR. Molecular Modeling: Principles and Applications. London: Longman Inc; 1996.
44. Onufriev A, Bashford D, Case DA. Exploring Protein Native States and Large-Scale Conformational Changes With a Modified Generalized Born Model. Proteins. 2004; 55:383–394. [PubMed: 15048829]
45. Ryckaert JP, Ciccotti G, Berendsen HJC. Numerical Integration of the Cartesian Equations of motion of a System With Constraints: Molecular Dynamics of N-Alkanes. J. Comput. Phys. 1977; 23:327–341.
46. Hayashi T, Zhuang W, Mukamel S. Electrostatic DFT Map for the Complete Vibrational Amide Band of NMA. J. Phys. Chem. A. 2005; 109:9747–9759. [PubMed: 16833288]
47. Kubelka J, Keiderling TA. Ab Initio Calculation of Amide Carbonyl Stretch Vibrational Frequencies in Solution with Modified Basis Sets. 1. N-Methyl Acetamide. J. Phys. Chem. A. 2001; 105:10922–10928.

48. Hamm P, Lim M, Hochstrasser RM. Structure of the Amide I Band of Peptides Measured by Femtosecond Nonlinear-Infrared Spectroscopy. J. Phys. Chem. B. 1998; 102:6123–6138.
49. Baiz CR, Sam PC, Reppert MK, Jones KC, Tokmakoff A. Coherent Two-Dimensional Infrared Spectroscopy: Quantitative Analysis of Protein Secondary Structure in Solution. Analyst. 2012; 137:1793–1799. [PubMed: 22398665]
50. Torii H, Tasumi M. Model Calculations on the Amide I Infrared Bands of Globular Proteins. J. Chem. Phys. 1992; 96:3379.
51. Neria E, Fischer S, Karplus M. Simulation of Activation Free Energies in Molecular Systems. J. Chem. Phys. 1996; 105:1902.
52. Abramavicius D, Palmieri B, Voronine DV, Sanda F, Mukamel S. Coherent Multidimensional Optical Spectroscopy of Excitons in Molecular Aggregates; Quasiparticle versus Supermolecule Perspectives. Chem. Rev. 2009; 109:2350–2408. [PubMed: 19432416]
53. Chernyak V, Zhang WM, Mukamel S. Multidimensional Femtosecond Spectroscopies of Molecular Aggregates and Semiconductor Nanostructures: The Nonlinear Exciton Equations. J. Chem. Phys. 1998; 109:9587.
54. Zhang WM, Chernyak V, Mukamel S. Multidimensional Femtosecond Correlation Spectroscopies of Electronic and Vibrational Excitons. J. Chem. Phys. 1999; 110:5011.
55. Mukamel S. Multidimensional Femtosecond Correlation Spectroscopies of Electronic and Vibrational Excitations. Annu. Rev. Phys. Chem. 2000; 51:691–729. [PubMed: 11031297]
56. Zhuang W, Abramavicius D, Hayashi T, Mukamel S. Simulation Protocols for Coherent Femtosecond Vibrational Spectra of Peptides. J. Phys. Chem. B. 2006; 110:3362–3374. [PubMed: 16494351]
57. Humphrey W, Dalke A, Schulten K. VMD: Visual Molecular Dynamics. J. Molec. Graphics. 1996; 14:33–38.
58. Bendova-Biedermannova L, Hobza P, Vondrasek J. Identifying Stabilizing Key Residues in Proteins Using Interresidue Interaction Energy Matrix. Proteins. 2008; 72:402–413. [PubMed: 18214960]
59. Culik RM, Serrano AL, Bunagan MR, Gai F. Achieving Secondary Structural Resolution in Kinetic Measurements of Protein Folding: A Case Study of the Folding Mechanism of Trp-cage. Angewandte Chemie-International Edition. 2011; 50:10884–10887.

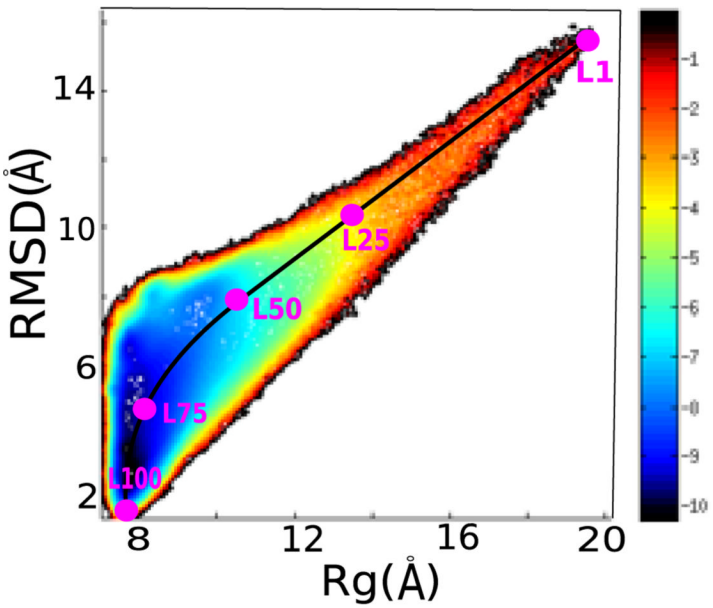

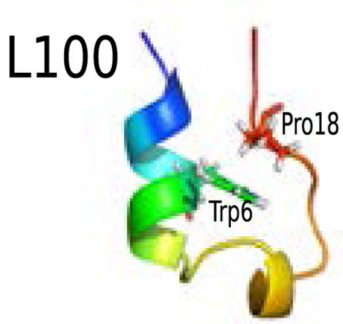

Figure 1.

Free energy profile of Trp-cage folding versus RMSD and R_g. (top). Five structures along the folding pathway are labeled L1, L25, L50, L75, and L100. The corresponding structures are shown (bottom). Trp6 and Pro18 are shown by stick representation.

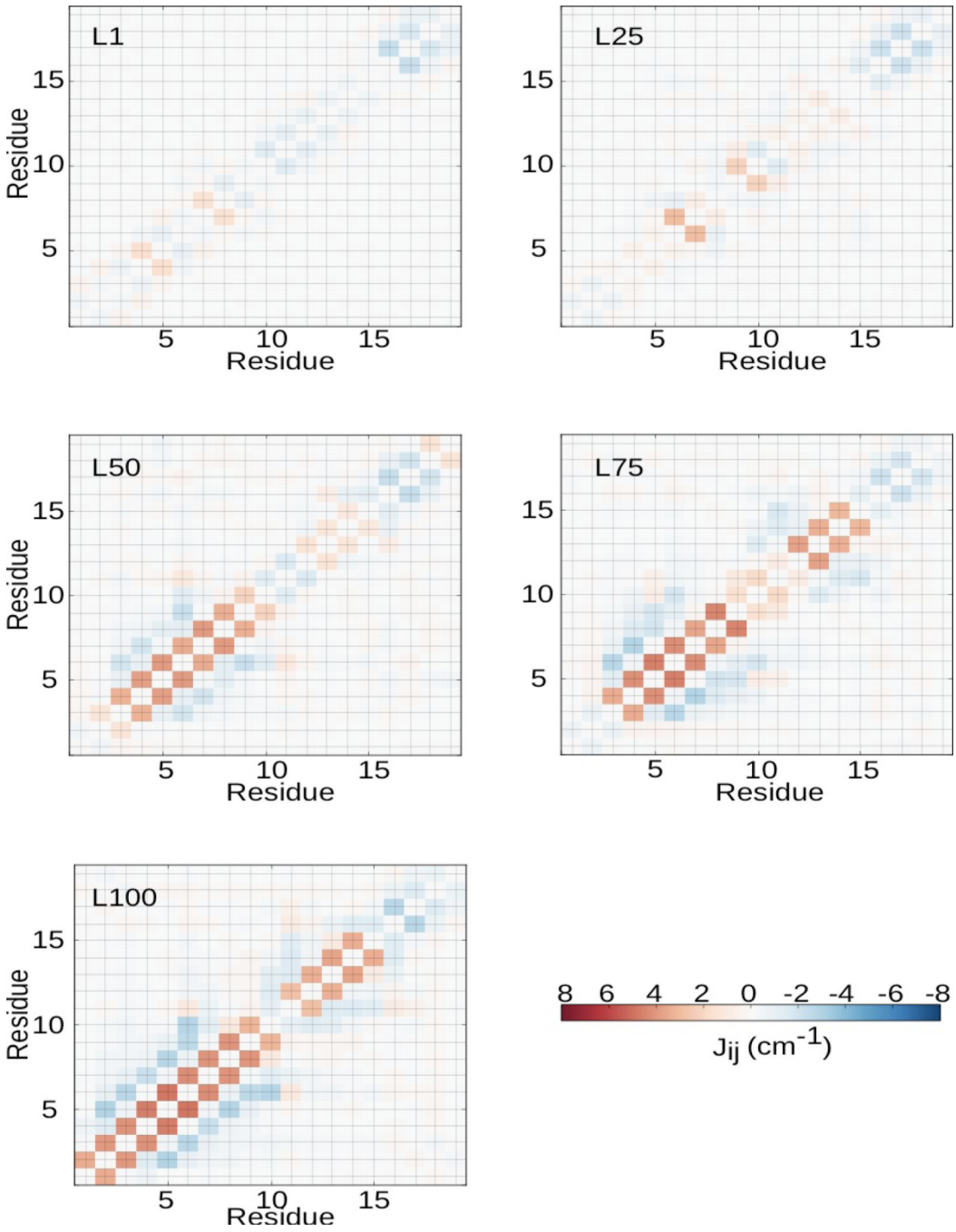

Figure 2.
Average transition dipole couplings among the different amide I vibrational modes for L1, L25, L50, L75, and L100.

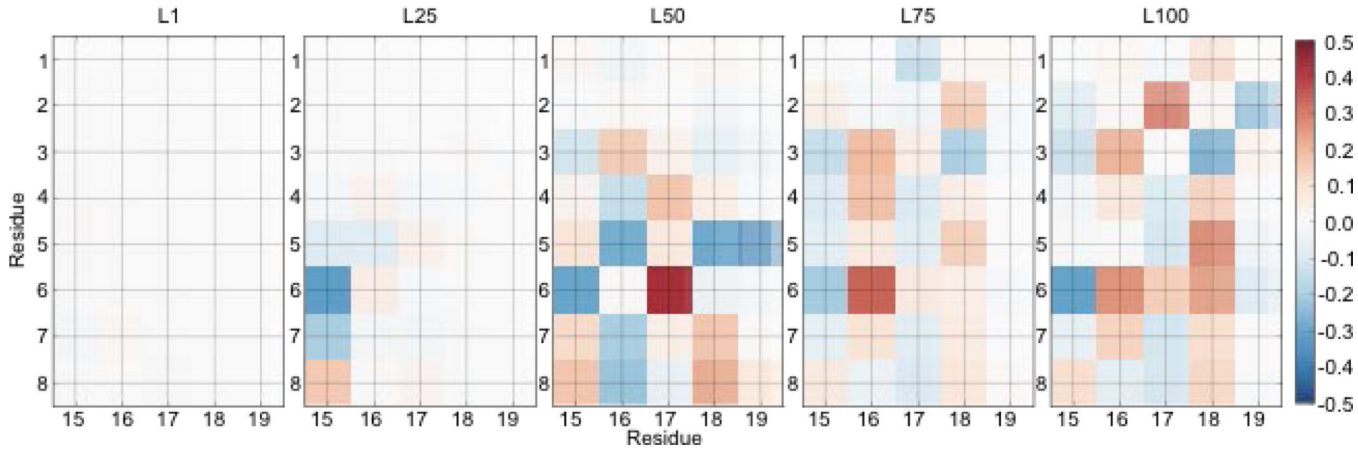

Figure 3.
Average coupling between residues 1–9 and residues 15–19 in cm^{-1}.

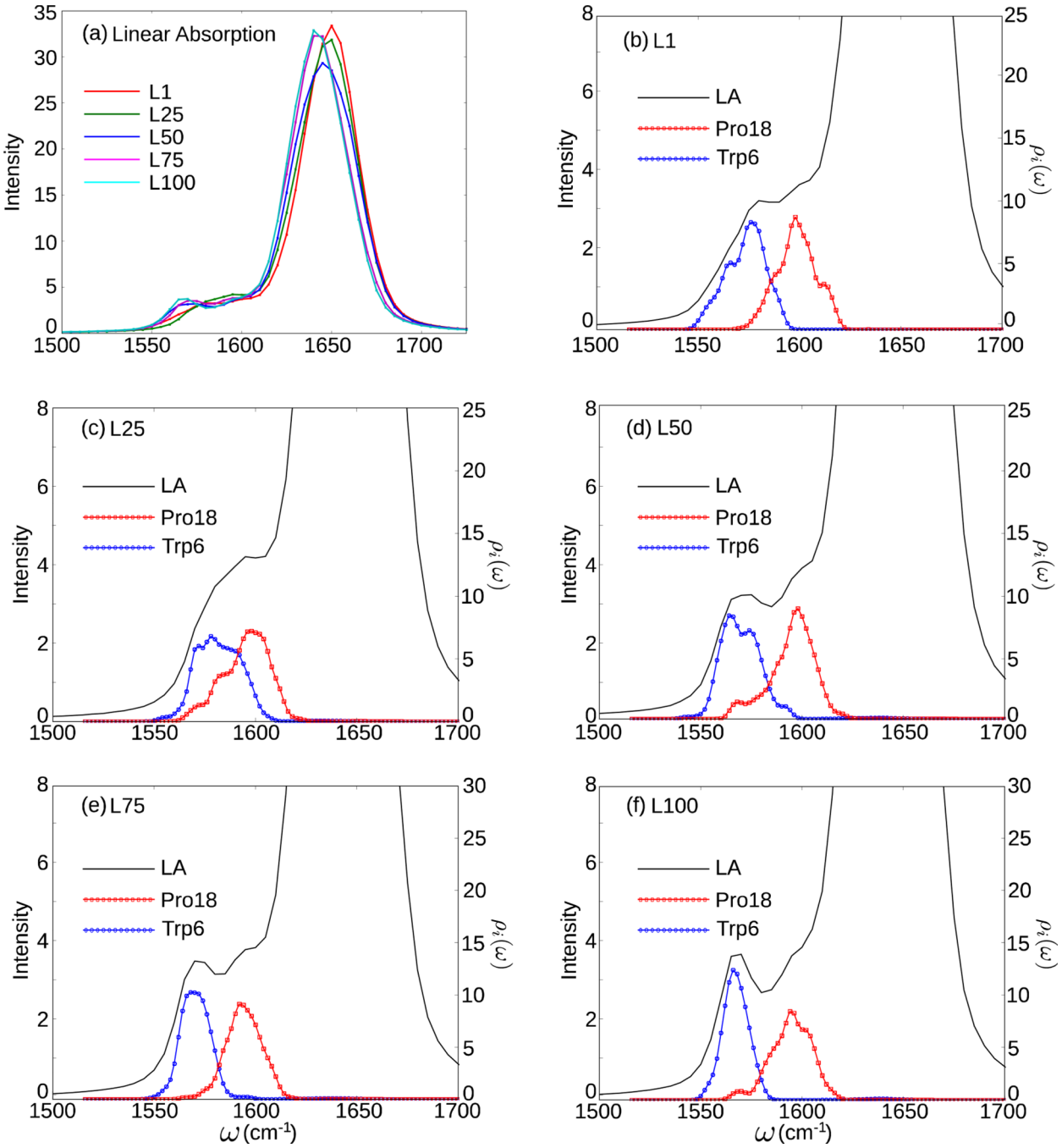

Figure 4.

(a) Amide I absorption spectra for L1, L25, L50, L75, and L100 where Trp6 and Pro18 are isotopically labeled. (b)–(f) Isotope-labeled region of the linear absorption spectra and projected density of states for L1, L25, L50, L75, and L100.

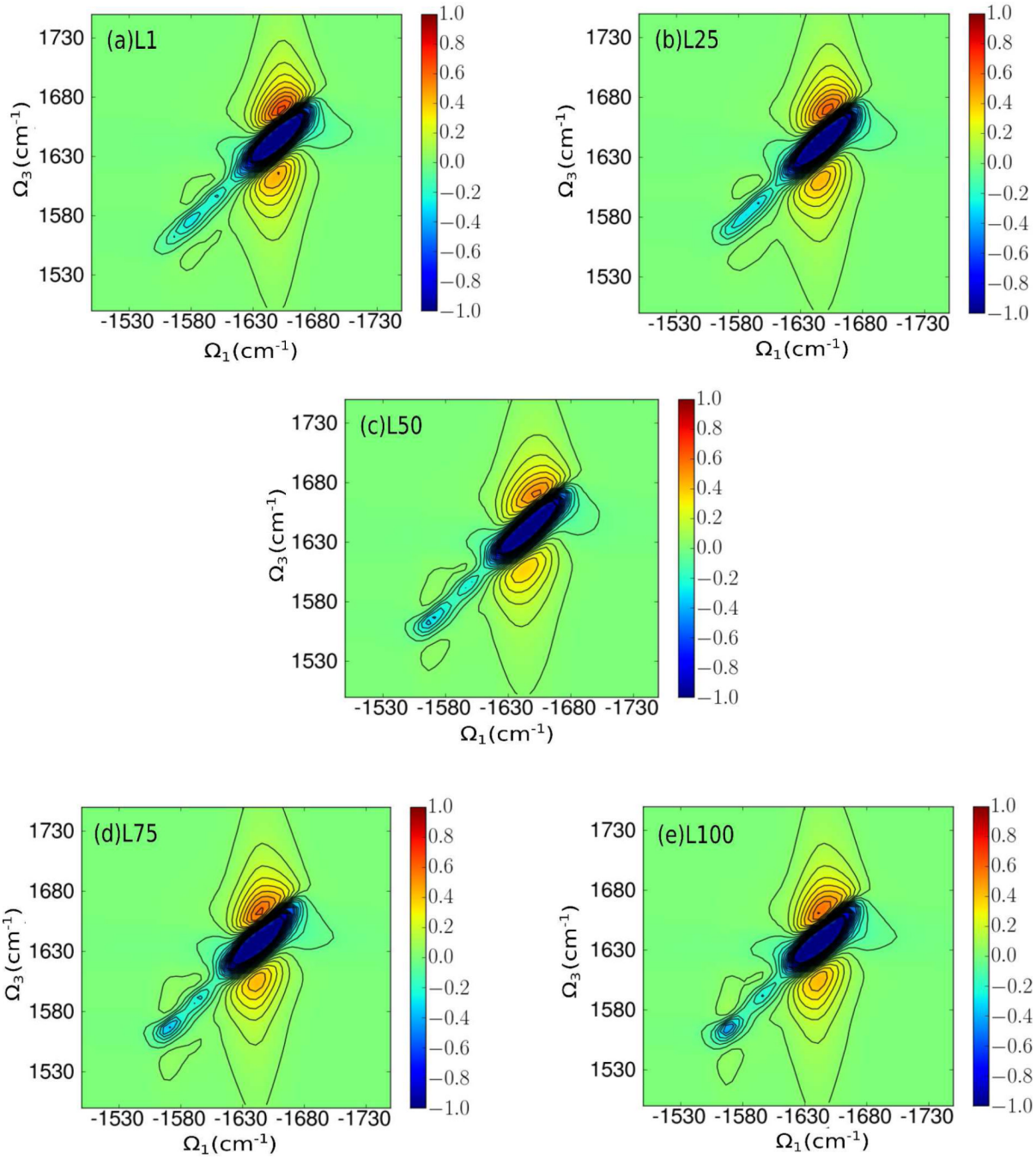

Figure 5.

Isotope-labeled nonchiral (*xxxx*) 2DIR $\boldsymbol{k}_{\mathrm{I}} + \boldsymbol{k}_{\mathrm{II}}$ amide I spectra for L1, L25, L50, L75, and L100. Trp6 and Pro18 are isotopically labeled.

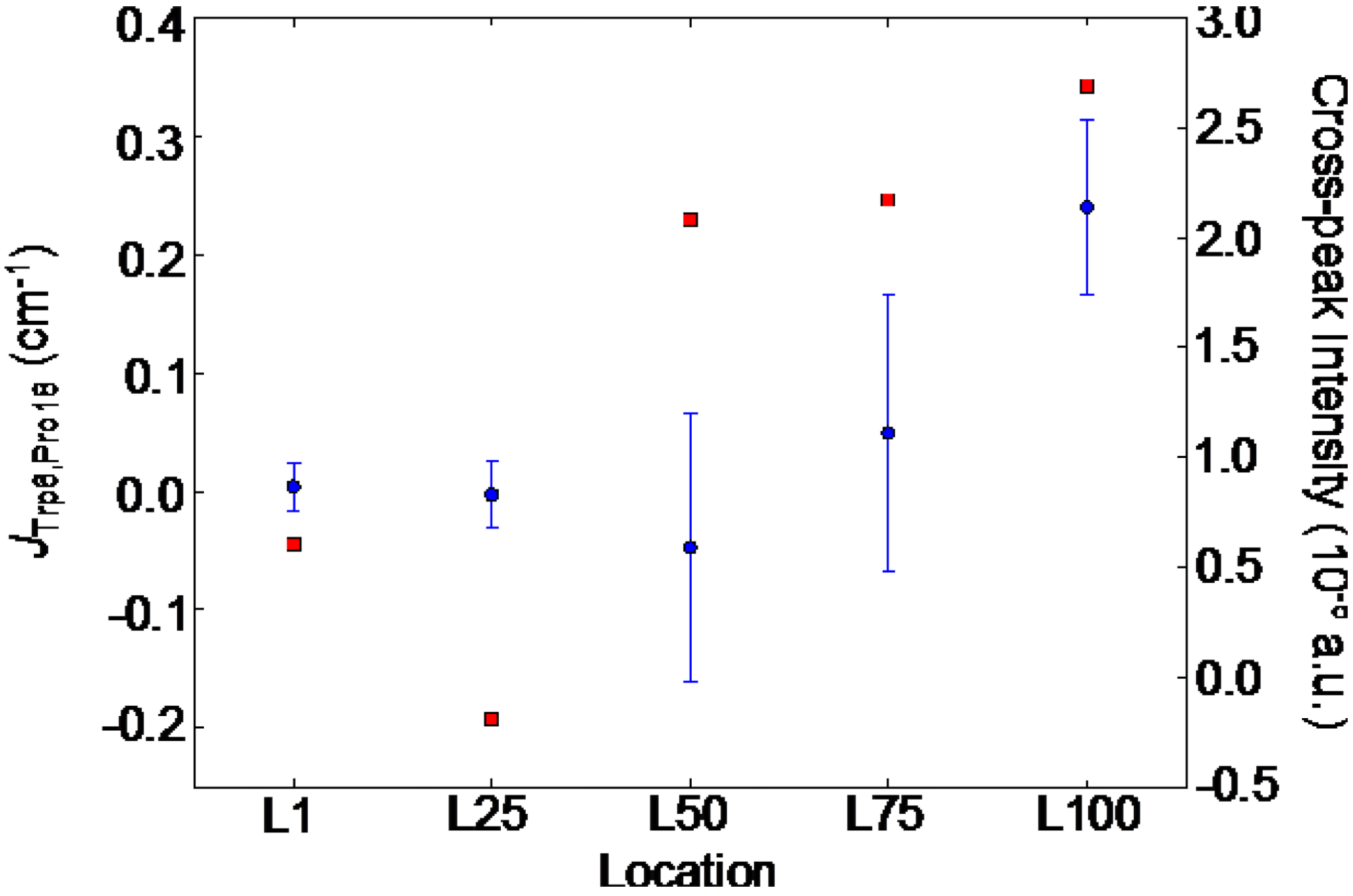

Figure 6.
Correlation plot of the coupling of Trp6 and Pro18 and the cross peak intensity. The average coupling is displayed along with the standard deviation in blue. The cross-peak intensities are displayed in red.

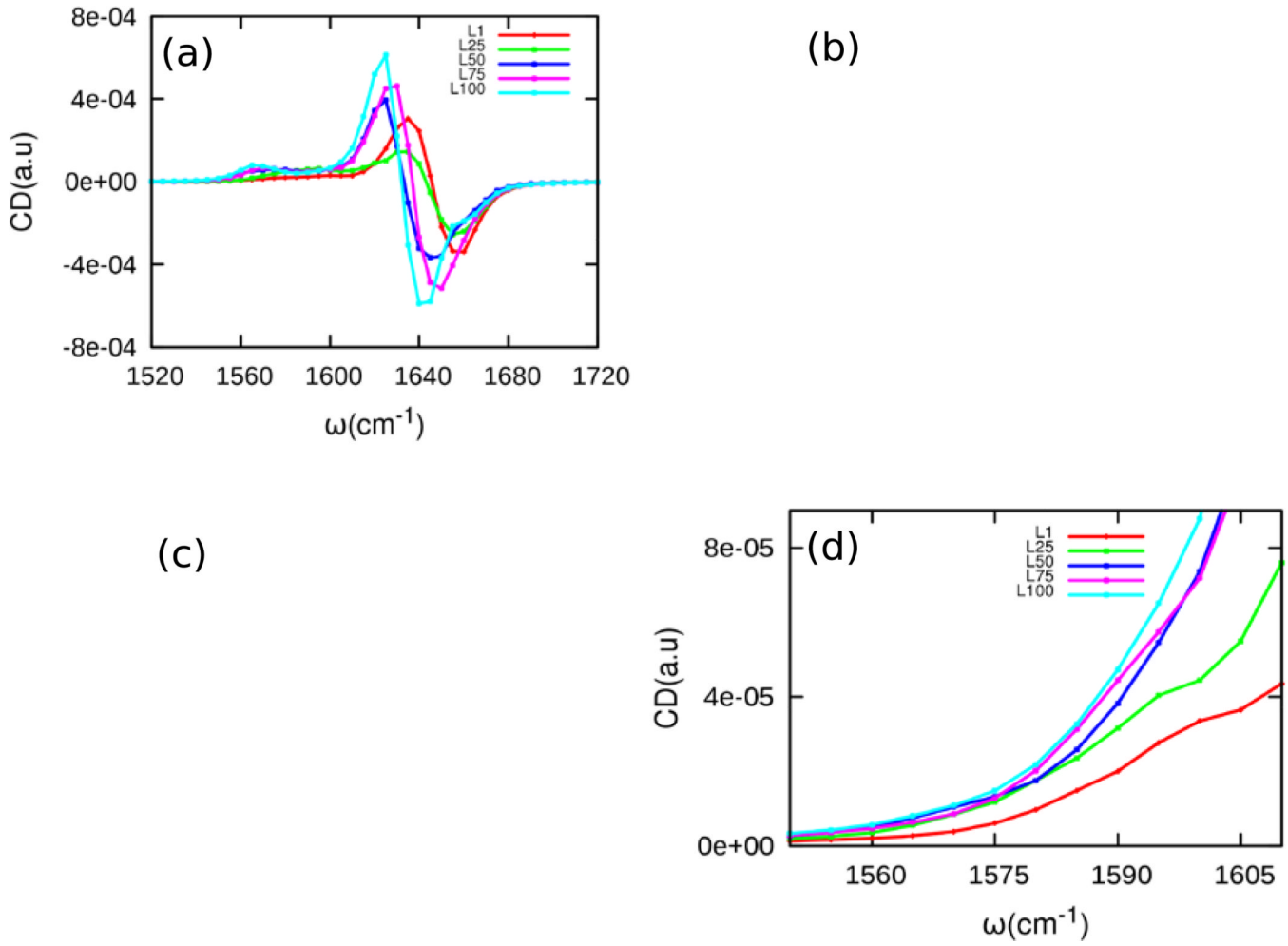

Figure 7.

(a) VCD spectra for L1, L25, L50, L75, and L100 with Trp6 and Pro18 both isotopically labeled. (b) Isotope-labeled region of the vibrational circular dichroism spectra with Trp6 and Pro18 both labeled. (c) Isotope-labeled region of the VCD spectra with only Trp6 labeled. (d) Isotope-labeled region of the VCD spectra with only Pro18 labeled

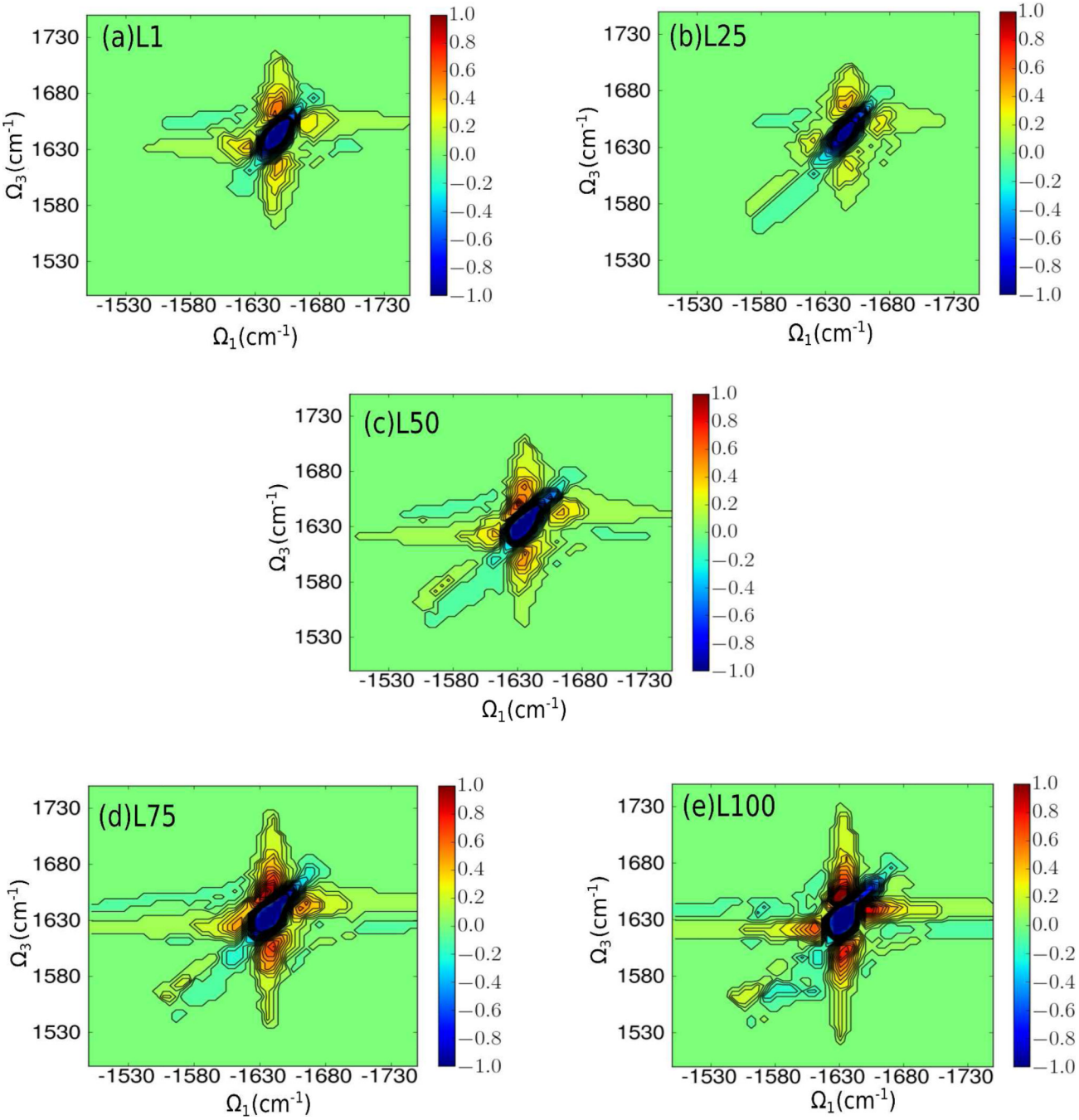

Figure 8.
Isotope-labeled chirality-induced (*xxxy*) 2DIR spectra for L1, L25, L50, L75, and L100.

Table 1

The average number of hydrogen bonds of the whole peptide and its parts for L1, L25, L50, L75, and L100. The hydrogen bonds were calculated using VMD [57] with an acceptor-donor distance cutoff of 3.5 Å and an acceptor-donor-hydrogen angle cutoff of 30 degrees. Residues 1–9, 10–14 and 15–19 were defined as the α-helix, "other", and coil region, respectively, to calculate the corresponding hydrogen bonds. Intra α-helix includes hydrogen bonds among the α-helix region and inter α-helix includes hydrogen bonds between the α-helix region and all other residues.

Location	Whole peptide	Whole α-Helix	Intra α-Helix	Inter α-Helix	Coil	Other
1	0.89	0.62	0.58	0.04	0.23	0.14
25	2.27	1.65	1.06	0.58	0.57	0.73
50	6.12	4.84	1.95	2.88	3.49	1.27
75	7.76	5.22	2.56	2.66	3.70	2.81
100	8.33	5.48	3.03	2.45	2.82	3.34